PHYSICAL REVIEW E **71**, 035101(R) (2005)

Set of measures to analyze the dynamics of nonequilibrium structures

Girish Nathan* and Gemunu Gunaratne†
Department of Physics, University of Houston, 4800 Calhoun Blvd., Houston, Texas 77204, USA
(Received 27 April 2004; published 11 March 2005)

We present a class of statistical measures that can be used to quantify nonequilibrium surface growth. They are used to deduce information about spatiotemporal dynamics of model systems for spinodal decomposition and surface deposition. Pattern growth in the Cahn-Hilliard equation (used to model spinodal decomposition) are shown to exhibit three distinct stages. Two models of surface growth, namely, the continuous Kardar-Parisi-Zhang model and the discrete restricted-solid-on-solid model are shown to have different saturation exponents.

DOI: 10.1103/PhysRevE.71.035101 PACS number(s): 05.50.+q, 64.75.+g, 05.40.−a, 05.70.Np

Analysis of pattern forming processes [1–10] require statistical characterizations because the detailed structure of patterns typically depends on uncontrollable factors such as the precise initial state and stochastic effects. Although measures such as the structure factor, correlation length, and roughness have been used to provide statistical descriptions of patterns, there are many additional facets that are not uniquely captured by these measures [11]. The absence of a sufficiently broad array of statistical measures also makes it difficult to identify the consequences of specific phenomena, such as the role played by stochasticity in spatiotemporal dynamics. In this paper, we present a family of characteristics, $\mu(\beta,t)$, that are derived from the contours of a given structure.

Consider two models of surface growth. One is the continuous Kardar-Parisi-Zhang (KPZ) model, and the second is the discrete restricted-solid-on-solid (RSOS) model. Commonly used statistical measures to analyze surface growth and patterns include surface roughness (i.e., the standard deviation of the heights), $W_L(t)$, where L is the lattice size and t the time, the correlation length [8], and the mean domain size [12,13]. For the KPZ and RSOS interfaces, $W_L(t)\sim t^{\theta}$ when $t\ll L^z$. At very large times, $W_L(t\to\infty)\sim L^{\alpha}$ [8]. The growth exponent θ, the dynamic exponent z, and the roughness exponent α, depend only on the dimensionality of the growth process and are independent of L apart from finite-size scaling corrections [6]. It has been found numerically that these exponents are the same in all dimensions for the KPZ and the RSOS models. Based on the results, it has been asserted that KPZ and RSOS belong to the same universality class, although tilt-dependence studies [14] have been used to establish differences between them. One use of the availability of additional statistical measures is to test the validity of such assertions. One of our conclusions is that there are statistical features that are not common to KPZ and RSOS models.

Nonequilibrium pattern formation and dynamics have also been extensively studied in the context of spinodal decomposition using the Cahn-Hilliard equation [1,12,13]. Their spatiotemporal dynamics have been classified into two regimes—an early stage where there are many small clusters (cluster size $\ll L$) and a late stage where there are large interconnected domains and cluster sizes are comparable to L. The mean domain size in the late phase is found to grow in time with an exponent $\frac{1}{3}$ [13].

Consider a planar pattern represented by a scalar field $U(\vec{x},t)$, which can be the height of an interface, or some relevant intensity field. One feature not captured by the correlation length and roughness is the curvature field of the contour lines of U. The possibility of using curvature for such an analysis has been proposed before [11,15–19], but in practice the results are very sensitive to noise. The underlying reason is that the evaluation of $\kappa=(U_{xx}U_y^2+U_{yy}U_x^2-2U_{xy}U_xU_y)/(U_x^2+U_y^2)^{3/2}$ is very sensitive to errors in calculating the denominator. In place of κ, one can use another measure, namely, the determinant of the Hessian normalized by the variance of U, $\Delta=(U_{xx}U_{yy}-U_{xy}^2)/\mathrm{Var}(U)$. Unlike κ, the calculation of Δ is fairly insensitive to noise. Further, for typical local structures, Δ is proportional to κ.

The measures we define are

$$\mu(\beta,t)=\left(\frac{\int d^2\vec{x}|\Delta|^{\beta}}{\int d^2\vec{x}}\right)^{1/4\beta}. \qquad (1)$$

Note that for each β, $\mu(\beta,t)$ has dimensions of inverse length. Furthermore, the measures $\mu(\beta,t)$ are invariant under all rigid Euclidean transformations (i.e., translations, rotations, and reflections) of a pattern. The use of moments, β, allows us to emphasize regions with different values of Δ, thereby providing an array of length scales associated with the structure. The use of multiple length scales is similar in spirit to using generalized dimensions [20,21] to characterize strange attractors, although the spatiotemporal nature of the dynamics for the models considered in this paper makes a further connection difficult. In our analysis, we define $\sigma(\beta,t)$ as the growth rate of $\mu(\beta,t)$, i.e., $\mu(\beta,t)\sim\exp[\sigma(\beta,t)t]$.

The organization of the paper is as follows. We first discuss the results of our analysis for the CHE, a paradigmatic model for spinodal decomposition. We describe distinct stages in the spatiotemporal dynamics using $\mu(\beta,t)$. We then proceed to analyze the KPZ and RSOS models and show that during the initial stage, $\mu(\beta,t)$ does indeed lend additional

*Electronic address: Girish.Nathan@mail.uh.edu
†Electronic address: Gemunu@mail.uh.edu

credence to the suggestion that in the strong nonlinear coupling limit, they do belong in the same universality class. However, our analysis of the late stage shows that the saturation exponents for the two models are different. The computational techniques used to obtain the data for these models is discussed in detail elsewhere [17] and will not be expanded upon here.

The CHE models spinodal decomposition using the dynamics of a conservative field $\psi(\vec{x},t)$ via

$$\frac{\partial\psi}{\partial t} = \frac{1}{2}\nabla^2(-\nabla^2\psi - \psi + \psi^3). \tag{2}$$

The Crank-Nicholson semi-implicit method [22] used to integrate Eq. (2) allows us to choose time steps as large as 0.4 and enables us to investigate the dynamics of the CHE to times large enough to observe saturation of $\mu(\beta,t)$, e.g., $T=4\,000\,000$ for the lattice size 512^2. An implicit integration scheme is used to integrate the partial differential equations. We deal with the nonlinear terms via a Taylor expansion to lowest order in $\delta\psi=\psi(t+\delta t)-\psi(t)$, and compute crossderivatives explicitly. For instance, a quadratic term $\psi^2(t+\delta t)$ is represented by $\frac{1}{2}[\psi^2(t)+\psi^2(t+\delta t)]$ in the semi-implicit scheme. On expanding to lowest order in $\delta\psi$, we find it is approximated by $\psi(t)\psi(t+\delta t)$. The mean values and error bars presented in the figures and text are obtained by averaging over 12 runs.

The dynamics of domain growth is as follows: Beginning from a random initial configuration, $|\psi(\vec{x},t)|$ and the domain size grow in time. For sufficiently large t, $\psi(\vec{x},t)$ reaches its equilibrium values of -1 or $+1$ [1,13]. The behavior of $\mu(\beta,t)$ is shown in Fig. 1(a). The dynamics can be separated into three stages. Initially, $\mu(\beta,t)$ appears to grow as a power law in time for about one-and-a-half decades, as seen in Fig. 1(a). There is a formation of small domains from the random initial field. As seen from the uppermost curve of Fig. 1(b), the growth rates $\sigma_1(\beta,t)$ for all β are nearly identical and independent of t. During this stage, one contribution to $\mu(\beta,t)$ comes from points near the domain boundaries. Although the growth of domains reduces the number of interfacial points, this decrease is countered by the fact that $|\psi(\vec{x},t)|$ has not saturated, and hence there are contributions to $\mu(\beta,t)$ from internal points. As a result, $\mu(\beta,t)$ increases during this stage.

The crossover between stages 1 and 2 occurs when the field ψ begins to saturate to its equilibrium values. A histogram of interfacial heights clearly shows the concentration near the equilibrium values of ±1. In stage 2 (lasting an order of magnitude in time), interior points of a domain make no contributions to $\mu(\beta,t)$. As a result, the aforementioned decrease in interfacial points now leads to a decrease in $\mu(\beta,t)$. The slopes $\sigma_2(\beta,t)$ in this stage are plotted in Fig. 1(b). We find that in this stage, the distinct moments relax at different rates [i.e., $\sigma_2(\beta,t)$ is β dependent]. Moreover, it is seen that the rate of relaxation of the larger moments is smaller than that for the lower moments. Thus, straightening of a relatively smooth domain boundary wall occurs at a faster rate than changes in sharper features. Running averages reveal that $\sigma_2(\beta,t)$ is uniform until the end of this stage. Observe

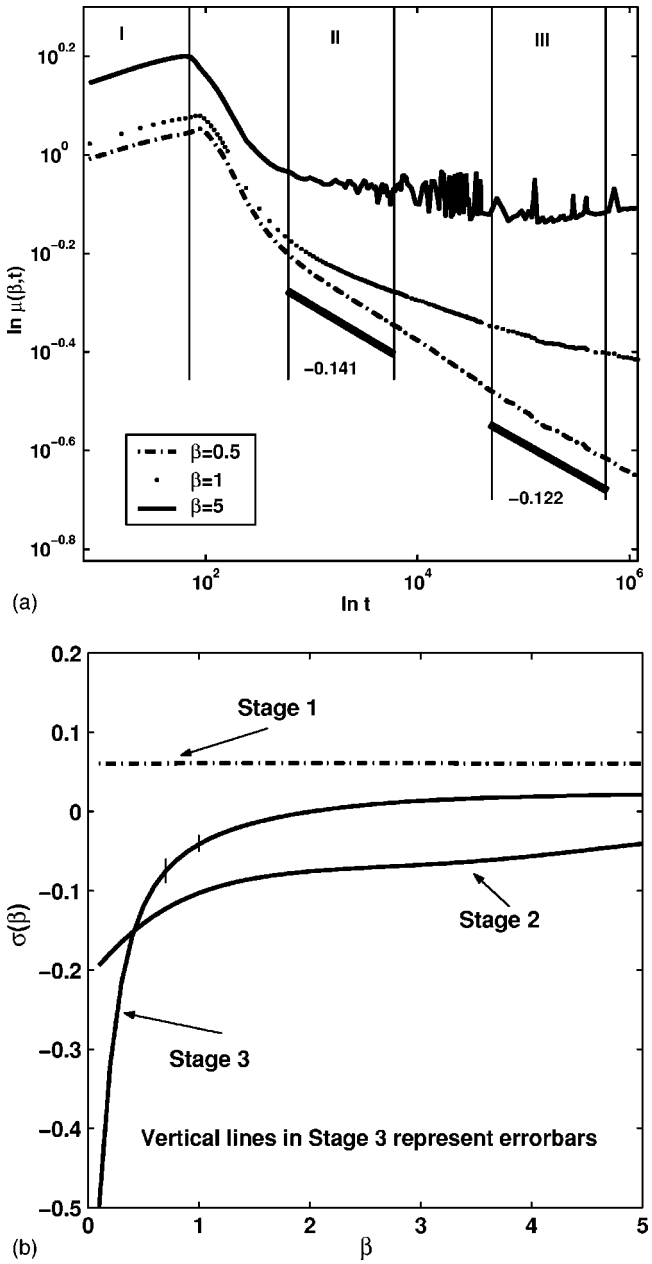

FIG. 1. Plots of the measure in time for various moments. $L=512$. (a) The noise-free case for different β. I, II, and III correspond to stages 1, 2, and 3. (b) The slopes vs β for stages 1, 2, and 3 for the noise-free case.

one critical difference between stages 1 and 2, namely, that the difference in relaxation of the distinct length scales cannot be determined without multiple measures.

The domain size as measured from the two-point correlation function [13] becomes comparable to L between stages 2 and 3 and $\sigma_2(\beta,t)$ changes during the transition. The spatiotemporal dynamics beyond this involves a coarsening of the large domains and elimination of the small ones. The disappearance of small domains can be identified by peaks in $\mu(\beta,t)$ for large values of β. These peaks result from the increase of local curvature during the disappearance of a domain. Figure 2 shows the effect of such an event on $\mu(\beta,t)$. It is clear that the elimination of a domain is accompanied by

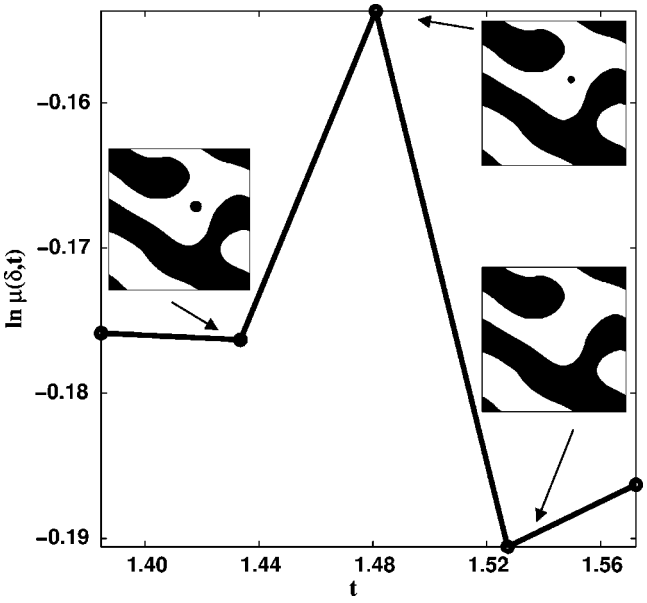

FIG. 2. Bubble disappearance for the $L=512$ lattice. The actual time is obtained by scaling the x-axis values by a factor 10^5. Notice how the peak in the measure corresponds to the bubble disappearing at approximately time 148 000. This is for $\beta=3.4$.

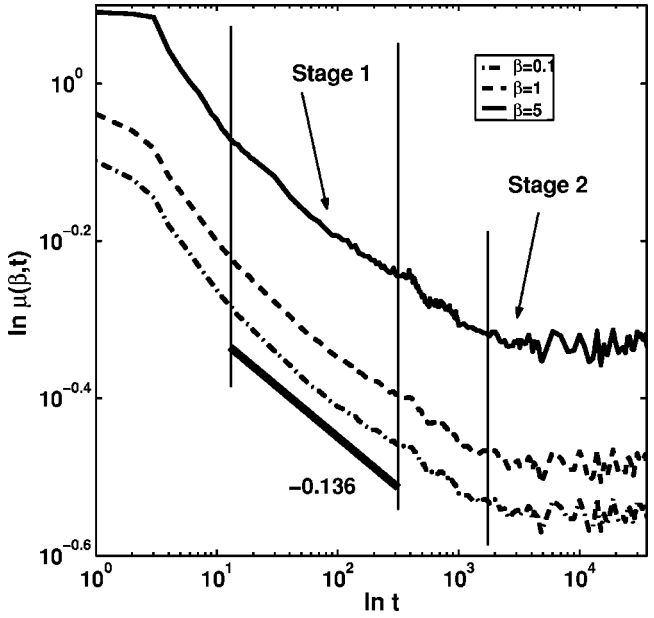

FIG. 3. Measure for the KPZ model for different β. $L=512$.

a peak in $\mu(\beta,t)$. The decay rates $\sigma_3(\beta,t)$ for the third stage vary more than the others, as seen from the error bars in Fig. 1(b). The error bars for the other stages are very small. However the general form of $\sigma_3(\beta,t)$ is the same; there is a β dependence for small values but a saturation for higher values of β. At the end of stage 3, only a handful of large domains remain; the only dynamics beyond this is an extremely slow straightening of the interfaces. A final dynamics involves saturation of $\mu(\beta,t)$ with the approach to "true equilibrium."

Surface roughness and domain size cannot provide such detailed information on the spatiotemporal dynamics. For a given structure, $W_L(t)$ saturates at the end of stage 1, and there is no discernible difference beyond this. The domain size grows as $R(t)\sim t^{1/3}$ at large times but also saturates between stage 2 and 3. When zero-mean external noise (amplitude $\sqrt{\epsilon}=10^{-6}$), we find that the dynamics in stage 3 is faster than in the noise-free case, i.e., $|\sigma_3(\beta,t)|$ is larger for the noisy dynamics. We also find that the saturation time of $\mu(\beta,t)$ is proportional to $\sqrt{\epsilon}$. We have also observed a similar behavior for conserved noise [12].

The KPZ equation is a paradigmatic model of nonequilibrium interfacial growth in the presence of lateral correlations [2,7]. The rescaled version of the KPZ equation [23] gives the dynamics of the height profile $h(\vec{x},t)$ at position $\vec{x}$ and time t as

$$\frac{\partial h(x,t)}{\partial t}=\nabla^2 h+\sqrt{\lambda}(\nabla h)^2+\eta(\vec{x},t). \tag{3}$$

Here $\sqrt{\lambda}$ is the parameter controlling the nonlinear term. $\eta(\vec{x},t)$ is δ-function-correlated noise of zero mean, which represents a random particle flux. RSOS is a discrete counterpart of the KPZ. Here, particles are added to a randomly chosen site i only if the addition ensures that all nearest-neighbor height differences $|\Delta h|\leqslant\Gamma$, where Γ is some predetermined positive integer.

Roughness and correlation function analyses of the dynamics of both KPZ and RSOS models show that their growth and roughness exponents take similar values in all dimensions, i.e., they are in the same universality class for sufficiently large values of λ ($\lambda\geqslant 15$). In the initial stages, the correlations spread across the entire lattice and the correlation length $\zeta\sim t^{1/z}$, where $z\sim 1.6$. It has been established numerically [23] that the strong nonlinear coupling limit of KPZ corresponds to the RSOS model in terms of the growth and saturation exponents of the surface roughness.

The behavior of $\mu(\beta,t)$ for the KPZ model ($L=512$) is shown in Fig. 3. The dynamics is qualitatively similar to the behavior of the surface roughness, and can be divided into two distinct stages. In stage 1, the lateral correlations spread across the entire lattice and we find that $\mu(\beta,t)$ decreases as $t^{-\sigma_1(\beta,t)}$ where $\sigma_1(\beta,t)$ is independent of β and t within numerical errors. The crossover between stages 1 and 2 signals the saturation of the roughness. The plots labeled by the dotted, dashed, and solid lines in Fig. 4 correspond to $\sigma_1(\beta,t)$ for $\lambda=1$, $\lambda=2$, and $\lambda=25$, respectively. $\mu(\beta,t)$ for the RSOS model exhibits a similar behavior during stage 1. In Fig. 4, the plot with circles shows $\sigma_1(\beta,t)$ versus β for the RSOS model. This corroborates the assertion that for the large λ limit, KPZ corresponds to the RSOS model in terms of the growth exponents, since it is seen clearly that $\sigma_1(\beta,t)$ for KPZ with $\lambda=25$ and for RSOS are within the error bars.

In stage 2 of Fig. 3, $\mu(\beta,t)$ saturates to a L-dependent value [given by $L^{\gamma(\beta)}$] where $\gamma(\beta)$ is the saturation exponent. However, in this case, we find that $\gamma(\beta)$ for KPZ and RSOS models, even at strong coupling, are very different. For example, $\gamma(\beta)$ for the RSOS model is found to be $\gamma(0.1)=-0.137\pm0.004$, while that for the KPZ model ($\lambda=25$) is $\gamma(0.1)=-0.308\pm0.029$ when $\beta=0.1$. For $\beta=1.0$, the saturation exponent for RSOS is $\gamma(1.0)=-0.097\pm0.004$,

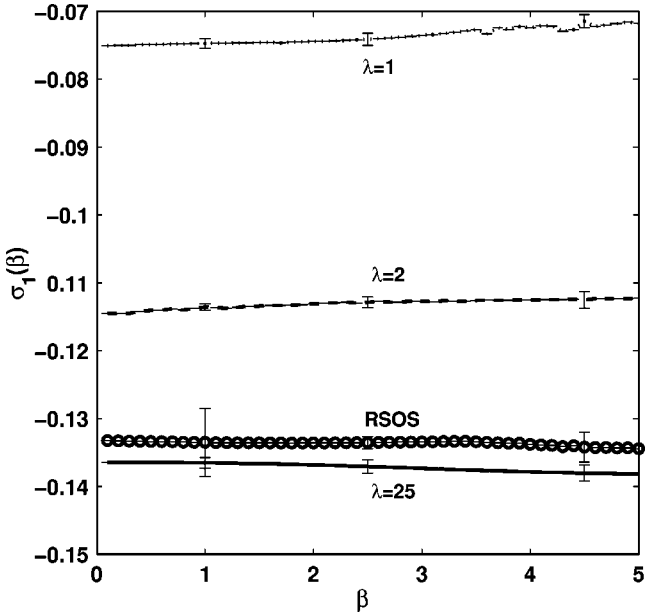

FIG. 4. The slopes vs β for various λ values compared with the RSOS slopes.

while that for the KPZ is $\gamma(1.0) = -0.213 \pm 0.005$.

In summary, we have presented a set of characteristics $\mu(\beta,t)$ that can be used to study spatiotemporal dynamics of systems represented by a scalar field $U(\vec{x},t)$. The measures represent statistical features of the contour field. At a given instant, $\mu(\beta,t)$ are a set of inverse length scales, and are defined in terms of the determinant of the Hessian of $U(\vec{x},t)$. Large values of β emphasize regions with larger curvature of contour lines.

The availability of a family of indexes allows us to provide a more comprehensive statistical description than is possible from individual measures. For example, it was shown for the CHE that during stage 2, relaxation of the distinct length scales associated with the structure occurs at different rates. This is very different from stage 1, where all such scales grow as $\mu(\beta,t) \sim t^{0.06}$. We are also able to identify instances where small domains of the pattern disappear by searching for peaks in $\mu(\beta,t)$ for large values of β.

Analysis of the KPZ and the RSOS models shows two stages in pattern evolution. For KPZ, $\mu(\beta,t)$ relaxes at a rate that depends on λ during stage 1. The rate of decay $\sigma_1(\beta,t)$ for large values of λ (typically $\lambda \geqslant 15$) is seen to be the same as for the RSOS model, thus reinforcing previous claims that both models belong to the same universality class. However, our analysis of surface contours provides an additional piece of information, namely, that all length scales $\mu^{-1}(\beta,t)$ associated with the spatiotemporal dynamics of these interfaces decay at the same rate. $\mu(\beta,t)$ saturates in stage 2 for both models, and the saturation value depends on the system size L as $L^{\gamma(\beta)}$. Interestingly, the function $\gamma(\beta)$ for the two models is different; after saturation, the structure of contours exhibit nonuniversal characteristics. It is thus possible to determine which of these models better represents the growth of an experimental interface.

The measures $\mu(\beta,t)$ can conceivably find applications in a diverse range of phenomena. Of particular interest is a quantitative description of the growth of epitaxially grown surfaces. Recently, a model has been proposed [24] that includes the free energy of mixing, phase-boundary energies, and concentration gradient dependent stress. Computations have shown several classes of far from equilibrium structures. In order to study effects of parameter variations, it is necessary to analyze the behavior of statistical quantities like $\mu(\beta,t)$. A study of this model is currently in progress.

The authors thank R. Rajesh and K. E. Bassler for a critical reading of the manuscript and for useful discussions. This research was partially funded by a grant from the National Science Foundation.

[1] A. J. Bray, Adv. Phys. **43**, 357 (1994).
[2] M. Kardar, G. Parisi, and Y.-C. Zhang, Phys. Rev. Lett. **56**, 889 (1986).
[3] J. M. Kim and J. M. Kosterlitz, Phys. Rev. Lett. **62**, 2289 (1989).
[4] M. C. Cross and P. C. Hohenberg, Rev. Mod. Phys. **65**, 851 (1993).
[5] J. S. Langer, *Solids Far From Equilibrium*, edited by C. Godreche (Cambridge University Press, Cambridge, 1992).
[6] F. Family and T. Vicsek, *Dynamics of Fractal Surfaces* (World Scientific, Singapore, 1991).
[7] T. Halpin-Healy and Y.-C. Zhang, Phys. Rep. **254**, 215 (1995).
[8] A.-L. Barabasi and H. E. Stanley, *Fractal Concepts in Surface Growth* (Cambridge University Press, Cambridge, 1995).
[9] S. D. Sarma and S. V. Ghaisas, Phys. Rev. Lett. **69**, 3762 (1992).
[10] S. D. Sarma, S. V. Ghaisas, and J. M. Kim, Phys. Rev. E **49**, 122 (1994).
[11] Y. Hu, R. Ecke, and G. Ahlers, Phys. Rev. E **51**, 3263 (1995).
[12] R. Toral, A. Chakrabarti, and J. D. Gunton, Phys. Rev. Lett. **60**, 2311 (1988).
[13] A. Chakrabarti, R. Toral, and J. D. Gunton, Phys. Rev. B **39**, 4386 (1989).
[14] J. Krug, P. Meakin, and T. Halpin-Healy, Phys. Rev. A **45**, 638 (1992).
[15] G. H. Gunaratne, Q. Ouyang, and H. L. Swinney, Phys. Rev. E **50**, 2802 (1994).
[16] G. H. Gunaratne, R. E. Jones, Q. Ouyang, and H. L. Swinney, Phys. Rev. Lett. **75**, 3281 (1995).
[17] G. H. Gunaratne, D. K. Hoffmann, and D. J. Kouri, Phys. Rev. E **57**, 5146 (1998).
[18] J. Kondev, C. L. Henley, and D. G. Salinas, Phys. Rev. E **61**, 104 (2000).
[19] J. Kondev and C. L. Henley, Phys. Rev. Lett. **74**, 4580 (1995).
[20] H. G. E. Hentschel and I. Procaccia, Physica D **8**, 435 (1983).
[21] T. C. Halsey *et al.*, Phys. Rev. A **33**, 1141 (1986).
[22] W. H. Press, B. P. Flannery, S. A. Teukolsky, and W. T. Vetterling, *Numerical Recipes In C* (Cambridge University Press, Cambridge, 1995).
[23] J. G. Amar and F. Family, Phys. Rev. A **41**, 3399 (1990).
[24] W. Lu and Z. Suo, J. Nanopart. Res. **2**, 333 (2000).